UNIVERSITY OF CALIFORNIA SAN DIEGO

Tracing Life History Patterns of Pacific Grenadier (*Coryphaenoides acrolepis*) off Baja California with Otolith Microchemistry

A Thesis submitted in partial satisfaction of the requirements
for the degree Master of Science

in

Marine Biology

by

Adrian Castillo

Committee in charge:

Professor Octavio Aburto-Oropeza, Chair
Professor Andrew Barton
Professor Ryan Hechinger

2022

The Thesis of Adrian Castillo is approved, and it is acceptable in quality and form for publication on microfilm and electronically.

University of California San Diego

2022

DEDICATION

For my Mom and Dad.

TABLE OF CONTENTS

LIST OF FIGURES

LIST OF TABLES

ACKNOWLEDGEMENTS

This thesis is presented as if it is the work of a single individual, however it is more so the result of a culmination of advice, mentorship, and support that has been provided by my peers. First and foremost, I'd like to thank my colleague, Dr. Leticia Cavole for the years of mentorship that she has provided for me, particularly during my undergraduate as a budding marine scientist. Each member of the Aburto Lab has been a source of advice for both my research and career during my time there. The members of my committee have been integral to my success in graduate school and finishing this work. In addition, I'd like to thank Dr. Allen Andrews for his active interest in my project relating to one he had done years ago, allowing me access to his samples and data. Chris Russo at the Keck Lab in Oregon State University was integral to my data acquisition process, which I would've been completely lost with otherwise. Dr. Karin Limburg at SUNY-ESF has been a fantastic resource in guiding my methodological approach and will continue to support my career in research as my PhD advisor next fall. Lastly, I'd like to thank my family and friends who have provided an amazing support system for me, especially during a pandemic which has challenged my work and perseverance.

This work is in preparation for submission to publication in a journal to be decided. Castillo, Adrian; Cavole, Leticia M.; Andrews, Allen H. "Tracing Life History Patterns of Pacific Grenadier (*Coryphaenoides acrolepis*) off Baja California with Otolith Microchemistry" The thesis author was the primary investigator and author of this manuscript.

ABSTRACT OF THE THESIS

Tracing Life History Patterns of Pacific Grenadier (*Coryphaenoides acrolepis*) off Baja California with Otolith Microchemistry

by

Adrian Castillo

Master of Science in Marine Biology

University of California San Diego, 2022

Professor Octavio Aburto-Oropeza, Chair

Unravelling the elemental patterns and age of fishes using otoliths allow us to better understand their life history. Pacific grenadier (*Coryphaenoides acrolepis*) are a species of deep-sea macrourid fish commonly found in the North Pacific along the continental slope between depths of 200 to 2000 m. Tracking the life history patterns in deep-sea fish is inherently difficult, however, examinations into otolith microchemistry offers chronological insight into potential environmental and endogenous drivers of habitat use. Laser ablation-

inductively coupled plasma-mass spectrometry (LA-ICP-MS) was used to analyze the otolith microchemistry of 118 mature adult Pacific grenadier (*C. acrolepis*). Archived samples were collected in the Northeast Pacific Ocean, offshore of the Baja California Peninsula and nearshore to Isla Guadalupe, Mexico, between the years of 1967 and 1971. We quantified 12 elemental isotope ratios (^{7}Li, ^{11}B, ^{24}Mg, ^{26}Mg, ^{55}Mn, ^{31}P, ^{63}Cu, ^{65}Cu, ^{66}Zn, ^{86}Sr, ^{138}Ba, and ^{208}Pb) from the otolith core towards the dorsal edge for 104 samples. Based on the relationship between otolith transect ablation length and total length, ablation transects were divided into larval, settled, and mature stages. ^{31}P, ^{63}Cu, ^{65}Cu, and ^{66}Zn ratios decreased with distance from the core of the otolith, potentially reflecting a decrease in metabolic activity and somatic growth with age. ^{86}Sr and ^{138}Ba ratios both steadily increased across lifespan, indicating movement to saltier and higher ambient concentration waters with depth. ^{55}Mn, ^{86}Sr, and ^{138}Ba showed elevated ratios within the settlement stage, suggesting a shift in environment that possibly reflects the hypoxic conditions common to the Oxygen Minimum Zone. Samples collected near Isla Guadalupe exhibited greater ratios of ^{7}Li, ^{26}Mg, ^{63}Cu, and ^{208}Pb, whereas samples found offshore of Baja were greater in ^{11}B, ^{55}Mn, and ^{86}Sr, indicating differences between offshore and near island populations. Overall, element ratios varied only slightly between offshore Baja and Isla Guadalupe collection sites, with k-means clustering accurately reclassifying 62.5% of samples. In addition, age estimates for this sample set were found to be consistent with a previous age and growth study and improved estimates of Von Bertalanffy growth curve parameters with the inclusion of older and larger samples. Overall, otolith microchemistry appears to be an effective tool to detect ontogenetic and regional aspects of *C. acrolepis*. This information will be key to proper management of *C. acrolepis* with potential increased fishing pressure on deep-sea ecosystems.

INTRODUCTION

Macrourids, also known as rattails or grenadier, are the largest family of gadiformes and the most diverse group of fishes in the deep sea, consisting of over 300 species across 34 genera (Cohen et al., 1990). Present in every ocean from pole to pole, they are found between depths of 200 to 2000 m along the continental slope. Grenadier are generalist feeders— functioning as both active benthic predators and demersal scavengers. Using a well-developed set of chemoreceptors along the mouth and chin, grenadier travel long distances in search of food, with little observed vertical movement (Priede et al., 1990). Pacific grenadier (*Coryphaenoides acrolepis*) is one of the most common species of macrourid found in the North Pacific Ocean (Cohen et al., 1990). They are distributed across a wide range: spanning from the southern tip of Japan across the Bering Sea and stretching through Alaska, United States, to Baja California, México. Grenadier are rarely the target for commercial fishing due to their unpalatable meat, though, they are a common source of bycatch in bottom-trawls and some species have been considered and exploited for market use (Devine et al., 2012). *C. acrolepis* is of particular interest due to their relatively good edible qualities and abundance off the west coast of the United States (Matsui et al., 1990). Listed as an Ecosystem Component Species under the Pacific Coast Groundfish Fishery Management Plan, their stock is not actively managed (Pacific Coast Groundfish FMP. 2020). The *C. acrolepis* fishery is considered to be of moderate concern by the Monterey Bay Seafood Watch, with 111 tons caught in commercial non-hake groundfish fisheries in 2011, below the estimated over-fishing limit of 1,386 tons (Groundfish, US West Coast, 2014). However, they are likely vulnerable to extensive fishing pressure, due to their reportedly slow growth and long lives with age validated estimates as old as 72 years old (Andrews et al., 1999).

Coryphaenoides abundances in the northeast Pacific have been correlated to the abundance of epibenthic fauna, suggesting that populations are heavily influenced by bottom-up controls (Bailey et al., 2006). Carbon and nitrogen isotope analyses into the gut contents of two macrourids indicate that while grenadier are top predators amongst the benthos, a significant portion of their nutrition is derived from scavenged remains of epipelagic nekton (Drazen et al., 2008). Thus, grenadier populations are thought to be sustained partially by the supply of carrion at depth, and their abundance has been correlated with that of hake, a common nekton off California (Drazen et al., 2012). *C. acrolepis*, however, consume a higher proportion of benthic invertebrates in comparison to other macrourids (Tuponogov et al., 2008).

There exists limited information regarding the life histories of macrourids and other deep-sea fishes. Hatching from eggs that float up below the thermocline, they exist as planktonic larvae until settling close the benthos when they grow close to 8 cm total length, reaching maturity at about 50 cm (Matsui et al., 1990). Like similar species, *C. acrolepis* exhibit patterns of ontogenetic vertical migration to deeper waters, with individuals settling as deep as 3700 m with age (Cohen et al., 1990). This pattern is evidenced by the tendency for larger and older specimens to be collected at depth and has been confirmed by otolith stable isotope analysis indicating migration into deeper, colder waters (Lin et al., 2012, Massutí et al., 1995). The diet of *C. acrolepis* also suggests a shift in ontogeny, with younger individuals primarily consuming infaunal polychaetes and amphipods before preying upon larger squid, fish, and crustaceans as they grow older (Drazen et al., 2001). Seasonal migrations of macrourids are poorly understood, though some species have been shown to vary in size-class vertical distribution and feeding activity over the course of a year (Tuponogov et al., 2008; Orlov & Torkranov, 2008). Giant grenadier appear to exhibit lengthy horizontal migrations (up to 1000 km) off the Russian coast

of the North Pacific Ocean (Tuponogov, 1997). Tracking deep-sea fish populations and migrations is inherently difficult since many perish due to barotrauma after capture when brought to surface and thus cannot be tagged and recaptured. Attempts to track grenadier with ingested transmitters have been limited in range and incapable of following individuals across lifespan (Priede et al., 1990). Microscopic planktonic larvae moving through a vast ocean are extremely difficult to follow through conventional tracking methods. Grenadier larvae are especially rarely encountered and only a single larval *C. acrolepis* was collected after an extensive sampling effort (Matsui et al., 1990).

Fish otoliths, also known as ear stones, are an inert calcium carbonate structure that can be used to estimate and validate the age of fishes (Pannella 1971; Campana 1999; Campana & Thorrold 2001). Subsequently, these structures have generated many decades of age and growth studies for various species (Jones & Hynes 1950; Lough et al., 1981; Hoyer et al., 1985). As they accrete over the course of an individual's lifespan, otoliths grow with age, incorporating minor, trace, and major elements from the surrounding environment (Sturrock et al., 2012). These characteristics present a feasible method of studying the ontogeny of fishes, especially in the deep sea, where means of observation are limited (Campana, 2005; Gerringer et al., 2018). The annual periodicity of the growth rings of *C. acrolepis* are particularly clear and have been validated through lead-radium isotopic dating (Andrews et al., 1999).

Otolith microchemistry analyses are a promising methodology for tracking an individual fish's life history patterns, habitat use, and physiology (Sturrock et al. 2014; 2015; Thomas et al. 2017). The primary ion pathway into an otolith occurs through uptake within the gill and gut membranes into the blood plasma before entering the endolymph and biomineralizing into the otolith proteinaceous matrix (Thomas et al. 2017; Hüssy et al., 2021). Elements can be

incorporated into the crystal structure through random trapping, substituting for Ca, and binding to the organic matrix. The pathway into the otolith can vary between elements, with some elements such as Sr, Ba, and Pb being incorporated into the crystal and salt fraction, likely through environmental controls. Other elements such as P, Cu, and Zn, are incorporated into the protein fraction of otoliths via physiological processes. Depending on the pathway within a given environment, elements found in otoliths can be used as proxies to track patterns in migration and/or physiology across an individual's lifespan (Sturrock et al., 2015, Hüssy et al., 2021). The use otolith microchemistry to track migrations in marine fishes are most limited by an instrument's ability to measure low concentrations of elements with high spatial resolution (Sturrock et al., 2012).

Various techniques have been employed to study otolith microchemistry, including 2D elemental mapping, radiometric dating, and isotopic temperature reconstruction (Andrews et al, 1999, Limburg et al., 2007, Longmore et al., 2011). Laser ablation-inductively coupled-plasma mass spectrometry (LA-ICP-MS) is a widely used method for measuring elements found in a solid material. The technique operates across two primary machines: the laser and the mass spectrometer. A laser beam is focused on a surface to generate fine particles, often in spots or along a continuous line. The ablated particles are vacuumed out into a plasma torch, exciting the ions present within. They are then introduced to a mass spectrometer detector to generate data in counts per second (cps). This data can be used to calculate the concentration of elemental isotopes across the ablated region using standardized references (Russo et al., 1999). A wide variety of fields, from geochemical to biological study, have used LA-ICP-MS to observe the microchemical makeup of various materials with high spatial resolution. Fisheries scientists have

applied this technique to determine life history patterns in migration and growth for species such as trout, salmon, and cod (Palace et al., 2007, Sanborn et al., 2003, Serre et al., 2018).

Using LA-ICP-MS, we investigated the chemical makeup of otoliths found in *C. acrolepis* from the otolith core to the edge, corresponding with the natal origin to the time of capture. The primary research questions guiding this study are: [1] What can the microchemistry of *C. acrolepis* otoliths inform about their life history, particularly across life stages?; [2] Do these observed patterns correlate with expected environmental and physiological processes?; and [3] Does *C. acrolepis* otolith microchemistry vary between collection sites off Baja and Isla Guadalupe? In this study, we measured the elemental ratios to ^{43}Ca of 12 different elemental isotopes: ^{7}Li, ^{11}B, ^{24}Mg, ^{26}Mg, ^{55}Mn, ^{31}P, ^{63}Cu, ^{65}Cu, ^{66}Zn, ^{86}Sr, ^{138}Ba, and ^{208}Pb. Additionally, we estimated the age for *C. acrolepis* and expanded on previous growth parameters with the inclusion of larger and older specimens.

In general, we hypothesized that otolith element ratios associated with the environment would reflect patterns of ontogenetic vertical migration to deeper waters, possibly mirroring depth profiles (Table 1). ^{86}Sr and ^{138}Ba can be proxies for colder and more saline waters, and measured ratios were predicted to increase further from the core as the fish moved deeper (Heimbrand et al., 2020). ^{55}Mn is often associated with hypoxic environments and was anticipated peak some distance from the otolith core, in agreement with oxygen vertical profiles off Baja California (Papiol et al., 2017). Elements mostly associated with the proteinaceous fraction of otoliths were expected to reflect patterns of slowing metabolic activity and somatic growth with age. Therefore, ^{31}P, ^{63}Cu, ^{65}Cu, and ^{66}Zn were predicted to decrease with distance from the core. ^{7}Li, ^{86}Sr, ^{138}Ba, and ^{208}Pb: isotopes most associated with the crystal and salt fraction— and therefore potential proxies for environmental processes— are expected to differ

between our collection sites. Unravelling ontogenetic and regional patterns in Pacific grenadiers will be integral to guiding proper conservation strategies.

Table 1: Hypothesized proxies for 12 different elemental isotopes found within in otoliths.

Hypothesized Proxy	Environment (salinity, temperature, oxygen, e.g.)	Physiology (metabolic rate, somatic growth, e.g.)	Environment + Physiology
Isotope X	^{7}Li, ^{11}B, ^{86}Sr, ^{138}Ba, ^{208}Pb	^{31}P, ^{63}Cu, ^{65}Cu, ^{66}Zn	^{24}Mg, ^{26}Mg, ^{55}Mn

(Thomas et al., 2017; Heimbrand et al., 2020; Hussy et al., 2021)

MATERIALS & METHODS

1. Sample Collection and Processing

One hundred and eighteen *C. acrolepis* sagittal otoliths were provided courtesy of the Marine Vertebrate Collection at the Scripps Institution of Oceanography. Samples were collected from a series of 19 SIO research cruises conducted in the North Pacific Ocean between 1967 and 1971, which primarily used vertical setlines for specimen capture. Of the samples with location data, 59 otolith samples were collected from locations at least 30 km offshore of the coast of the Baja California Peninsula, whilst 46 of the samples were collected from nearshore locations off the east coast of Isla Guadalupe, Mexico (Fig. 1). Depths of collection for sample trawls ranged between about 1197 and 1993 m beneath the surface and did not differ significantly between the two locations. All individuals collected were primarily mature adults with sizes ranging from 50.6 to 87 cm in total length (TL). The sexes of 51 *C. acrolepis* samples were noted; 30 of which were male and 21 were female.

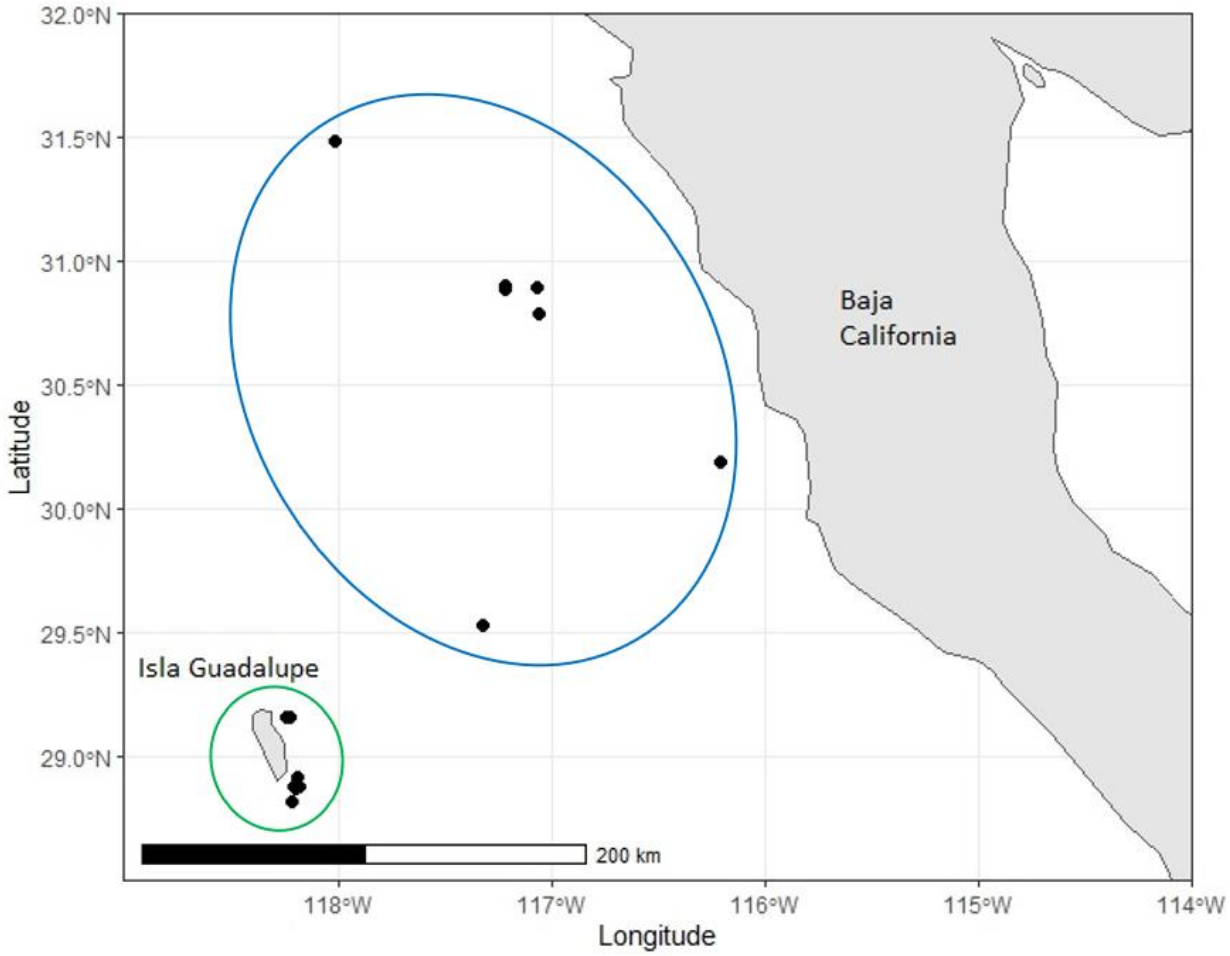

Figure 1: Map of 19 collection sites for SIO research cruises conducted between 1967-71. The blue and green ellipses indicate samples grouped into Baja California (n=59) and Isla Guadalupe (n=46), respectively. Vertical setlines were used to capture samples.

Otoliths were catalogued, photographed at 0.65 magnification, then weighed and measured in width, length, and thickness. They were placed in a silicon mold and embedded in a transparent epoxy resin. After allowing at least 24 hours the epoxy resin to harden, otoliths were removed from the mold and a precision diamond saw was used to cut transversal sections at the core of the otoliths about 0.7 mm thick. At least two thin sections were cut and examined under a microscope; the section with the most visible annual rings was selected for further analysis. Selected thin otolith sections were then polished with micromesh paper to increase ring clarity. Ages of individuals were estimated as the total number of annual rings visible when examined

under a compound microscope. Rings were counted starting from the core and following growth margins to the dorsal ridge. Age estimate data was combined with data from a previous study courtesy of Dr. Allen Andrews (Andrews et al., 1999). A von Bertalanffy growth curve was generated in RStudio v. 1.4.1103, combining the two datasets using the FSA package. In preparation for microchemical analysis, 118 sections were mounted on 11 microscope slides with double-sided tape.

2. LA-ICP-MS

For this study, a Photon Machine Analyte G2 Excimer laser and a Thermoscientific iCAP-RQ ICP-MS were used courtesy of the Keck Lab at Oregon State University. The laser operated with a spot size of 30 µm, a repetition rate of 10 Hz, energy at 75% (63.5 J/cm^2), and a scan speed of 10 µm/s. Each ablation line was manually charted on the system computer and the ablation length for each sample was noted. 14 samples were ablated continuously for the full length of the section, from the edge of the dorsal ridge, following growth margins to the core of the nucleus, then to the edge of the ventral ridge to assess symmetry. The other 104 samples were ablated from the ventral edge of the core to the dorsal ridge (Fig. 2). A NIST-612 standard was used as the primary standard for comparison and was ablated for about 60 seconds between each sample. A NIST-610 was used as the secondary standard and was ablated after every 5 samples. A MACS-3 standard was used as a safety standard and was ablated after every 10 samples. The elemental isotopes of ^{7}Li, ^{11}B, ^{24}Mg, ^{26}Mg, ^{43}Ca, ^{55}Mn, ^{31}P, ^{63}Cu, ^{65}Cu, ^{66}Zn, ^{86}Sr, ^{138}Ba, and ^{208}Pb were selected for measurement. The experiment ran over the course of three days to generate element profiles for all samples. All LA-ICP-MS data measurements were downloaded and stored in a .csv file format.

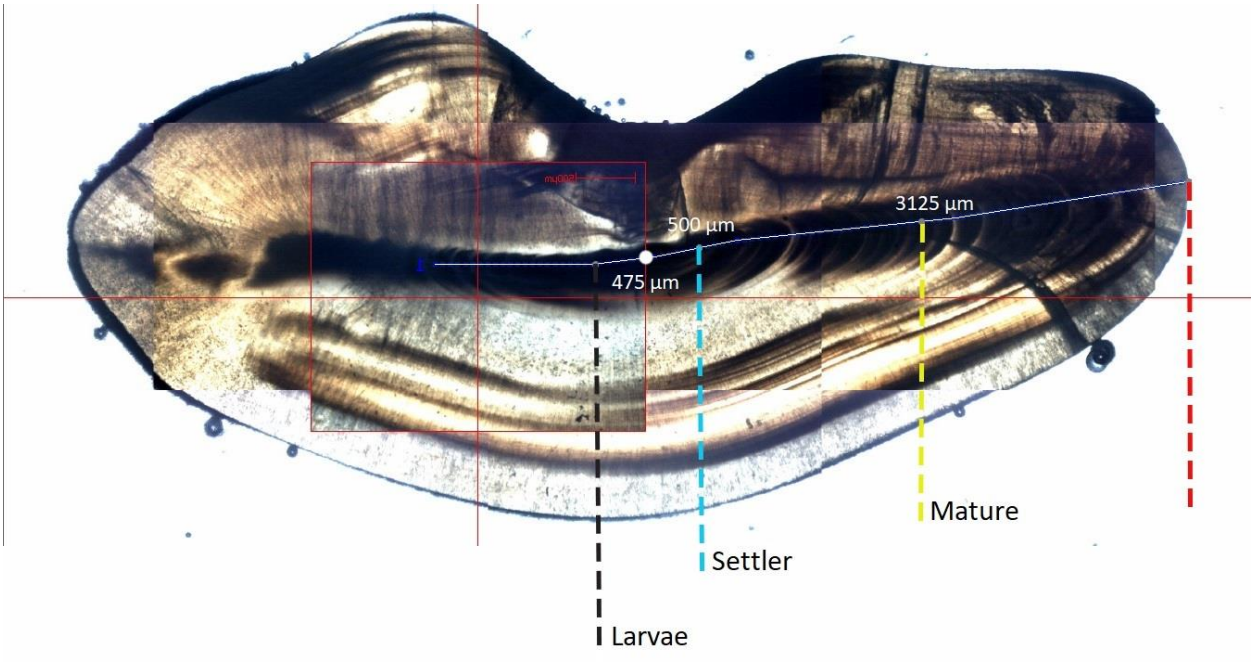

Figure 2: Example of a plotted ablation track for a thin transversal otolith section of *C. acrolepis*. The white line indicates the path of ablation, moving from the ventral edge of the core to the dorsal ridge. Life stage transitions from larvae to settlement (500 µm) and maturity (3125 µm) were defined relative to the estimated core (475 µm).

To calculate correction factors to derive isotope ratios, the average isotope counts per second (cps) values from NIST-612 ablations were calculated and ratioed to ^{43}Ca as the internal standard. The resulting values were multiplied by known NIST-612 concentrations ratioed to 71% CaO cited in Jochum et al., 2011 to get the m-correction factor for each element. Each calculated m-correction factor was averaged for NIST-612 ablations conducted between each slide. The following equation was used to calculate the final ratio for isotope *X*:

$$mol\ X/^{43}Ca\ = \left(\frac{X\ cps}{^{43}Ca\ cps}\right)\left(\frac{A_{r,standard}(X)}{A_{r,standard}(Ca)}\right)m$$

The resulting values were reported in mmol or µmol depending on the relative abundance of the isotope. This calculation was done for each cps value measured across the entire ablation length.

3. Quality Control Analysis

To evaluate the quality of isotope ratio measurements, multiple factors were considered. Samples with extremely high average isotope ratios were considered outliers per Tukey's definition and withheld from further analysis for that isotope. NIST-612 standards were run between each sample to account for measurement drift that may occur within the machine. To assess the precision of the NIST-612 ablation tracks, the standard deviation of isotope ratios along the ablation line for each standard was calculated. Precision was reported as the coefficient of variation of the normalized isotope ratios of each calculated using 11 separate NIST-612 standard ablation measurements. To assess measurement accuracy, a MACS-3 standard was ablated 11 times over the course of the experiment. The mean ^{43}Ca ratios of isotopes in the MACS-3 standards were calculated, then compared to the known values cited in Chen et. al, 2011 and reported as an average percent correlation. A two tailed t-test with inequal variances was also conducted between the known and recorded values. For the reported cps of each isotope of all otolith sample transects, the detection threshold for the ablation line was defined as 3 standard deviations above the mean of the background. This background mean was calculated as the mean cps between 3 and 19 seconds after the start of the laser run. The mean of the ablation line was calculated as the mean cps between 25 seconds after the start of the run and 30 seconds before the end of the run. This test was run for each isotope in all 118 samples and the percent success was reported. Sample isotope measurements which failed to pass the detection threshold were withheld from further analysis.

4. Quality Control Results

Overall, a general evaluation of all three quality control factors for the isotope data indicates mostly reliable results (Table 2). Based on our precision analysis, the ^{43}Ca ratios from the LA-ICP-MS across 11 NIST-612 standards did not vary greatly, with all isotopes but ^{24}Mg

having a coefficient of variation under 10%. Across all 12 isotopes, the average coefficient of variation was 4.64%, ranging between 1.31% and 13.12%. Isotope concentration measurements were mostly well correlated with known NIST-612 values, with all but 3 within 15% or their target value. ^{11}B, ^{31}P, and ^{208}Pb overshot their targets by a significant margin. The accuracy of ^{11}B is especially uncertain with an average NIST-612 element ratio 3.67 times the target value. For all 118 samples, most isotope ratios exceeded the detection limit: 3 standard deviations above the mean of the background. Three isotopes of note had lower percent success: ^{7}Li, ^{11}B, and ^{208}Pb had 12.71%, 17.80%, and 10.17% of samples fail to exceed the detection threshold, respectively.

The isotopes ^{11}B, ^{31}P, and ^{208}Pb failed to yield accurate NIST-612 measurements and may not reflect true values. However, while the calculated ratios are not necessarily accurate to the known values, they have been found to be precise, indicating that the error may be in the calculation of ratios rather than the raw data itself. Therefore, the trends visible in their associated figures can be considered substantial, though the isotope ratios are likely higher than the actual. Based on this analysis, element isotopes ^{26}Mg and ^{65}Cu were determined to be more reliable than their ^{24}Mg and ^{63}Cu isotopic counterparts. Elemental concentrations across distance for the 14 samples that were ablated the full length of the thin transversal section showed symmetry across the core for all isotopes (Fig. 3).

Table 2: Summary of LA-ICP-MS quality control analysis. Precision and accuracy are based on NIST-612 and MACS-3 measurements. The limit of detection was defined as 3 standard deviations above the mean of the background measurement. Extreme outlier data was excluded based on Tukey's definition.

Summary of Quality Control Analysis

Isotope:	^{7}Li	^{11}B	^{24}Mg	^{26}Mg	^{31}P	^{43}Ca	^{55}Mn	^{63}Cu	^{65}Cu	^{66}Zn	^{86}Sr	^{138}Ba	^{208}Pb	n
Precision														
Coefficient of Variation	4.32%	3.31%	13.12%	2.12%	4.57%	-	1.31%	3.03%	3.08%	5.29%	2.29%	4.43%	8.84%	11
Accuracy														
Average Percent Correlation	103.57%	367.24%	93.15%	98.30%	155.90%	-	101.93%	85.07%	96.92%	98.63%	94.47%	115.14%	138.36%	11
T-test p-value	0.0612	3.74E-08	0.000373	0.260	0.000356	-	0.563	0.00428	0.506	0.763	0.0401	0.0545	0.00362	11
Limits of Detection														
Percent Success	87.29%	82.20%	100%	100%	100%	100%	100%	99.04%	98.31%	100%	100%	100%	89.83%	118
Excluded Data														
Percent Excluded	22.12%	20.19%	15.38%	14.42%	1.92%	-	6.73%	8.65%	10.58%	5.77%	1.92%	1.92%	20.19%	104

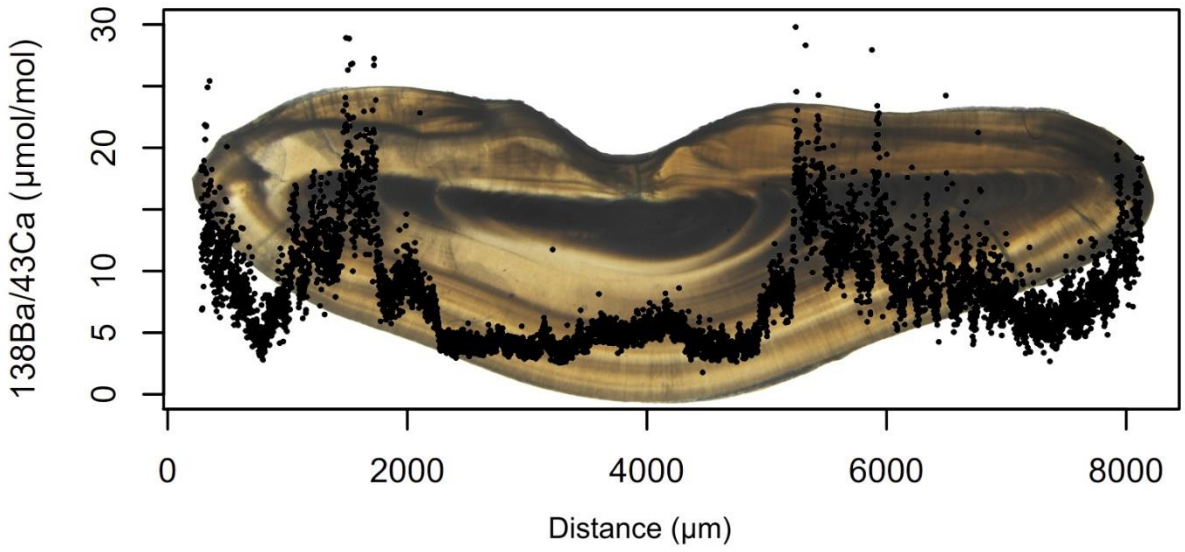

Figure 3: Measured $^{138}Ba/^{43}Ca$ ratios across an ablation line with a picture of the corresponding thin transverse otolith section sample transposed behind.

5. Statistical Analysis

All calculations and figure generation for statistical analysis were done in RStudio v. 1.4.1103 and Microsoft Excel. The 14 samples that were ablated from edge to edge of the thin transversal section were excluded from further analysis due their differing ablation patterns. After having calculated isotope concentration ratios across distance for 104 otolith transects, smoothed polynomial regression lines were generated using the loess() method in R with a smoothing span of 50%. Z-score normalization was used to standardize the data across all samples with the following equation:

$$X_{new} = \frac{X - \mu}{\sigma}$$

After standardizing the data, a final average regression line across all samples was plotted for each isotope. To estimate the distance of the core, the average distance to the first maxima across all samples and isotopes were used (475 µm), which coincides with the center of the

nucleus (Fig. 2). To calculate distances signifying the transition between life stages, the distance of the core was subtracted from all sample ablation lengths and a linear regression was plotted with those values against TL, assuming an isometric relationship ($y=0.016x$; $R^2 = 0.973$). With known TL values at settlement (TL = 8 cm) and maturity (TL = 50 cm), the respective distances along ablation tracks were calculated (Matsui et al., 1990). Using these transitionary distances separating life stages, the average ratios of each isotope and for each life stage were calculated and plotted in box-and-whisker plots.

In addition, a principal coordinate analysis (PCA) was conducted with the average life stage isotope ratios. Each element isotope represented a separate variable in the PCA. Chemical isotopes ^{24}Mg and ^{63}Cu were excluded from the PCA in favor of more accurate alternative isotopes ^{26}Mg and ^{65}Cu as determined through quality control evaluation. The imputePCA() method from the missMDA R package was used to predict null values which were excluded previously to account for data that were outliers or below the detection threshold. A corresponding biplot was generated to visualize the sample averages for each life stage across all isotopes between the first 2 dimensions.

The average ^{43}Ca ratios for each isotope were calculated for 33 samples collected off the coast of Isla Guadalupe and 57 samples found elsewhere off Baja California to test for spatial differences. A similar PCA was performed amongst this sample set between the two locations. In addition, the same dataset was clustered using k-means clustering with the kmeans() method in R. Two clusters were found to be most optimal for this data based on an evaluation of silhouette and gap statistics. The number of samples that were correctly grouped to the cluster that most corresponds to the collection site were divided by the total to calculate the reclassification accuracy to compare these clusters with the known location data. A two tailed t-test with inequal

variances was used to evaluate the difference in ratio between the two location categories for each isotope. Similarly, a t-test was conducted comparing the average isotope ratios of 30 male and 21 female samples to test for differences between sexes, though no significant differences were found for all isotopes.

RESULTS

1. Age, & Growth

Age estimates of individuals ranged between 20 and 72 years of age and appear to integrate well with age-length data from Andrews et al., 1999, despite being generally older and larger. The resulting von Bertalanffy growth curve and parameters ($L\infty = 76.7$; $k = 0.05605$; $t_0 = 1.142$) did not deviate greatly from Andrews et al. 1999, indicating that age readings for *C. acrolepis* are consistent and accurate (Fig. 4).

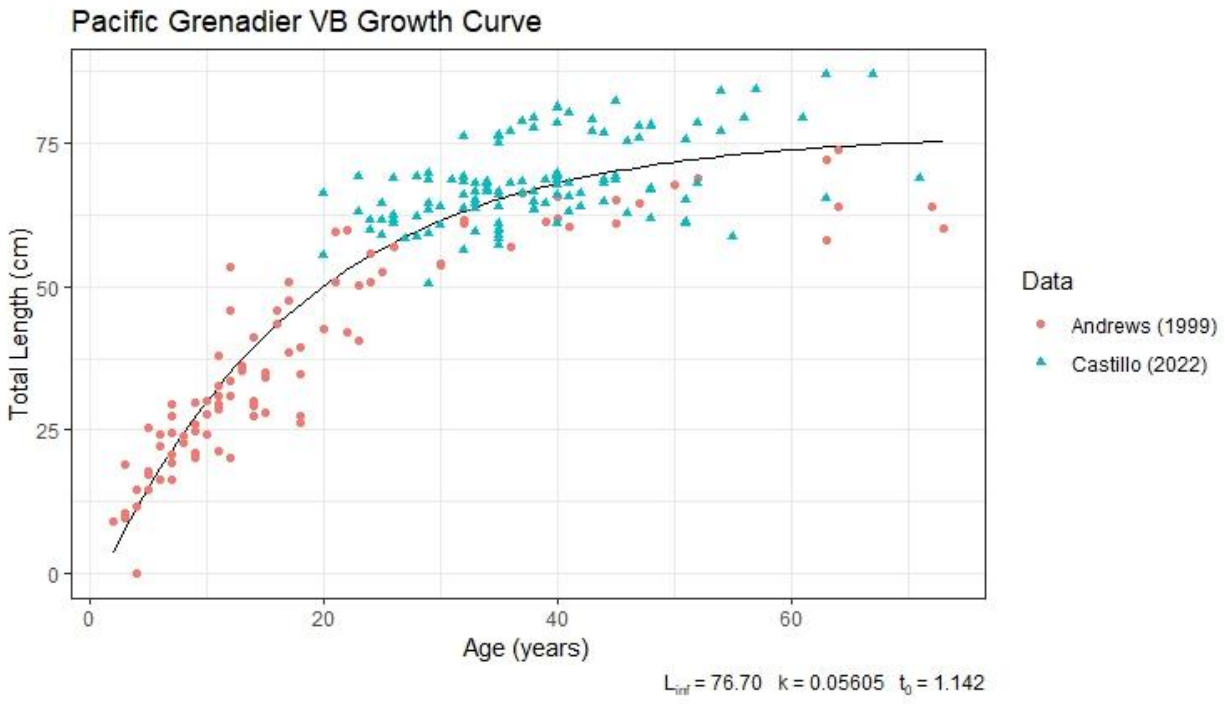

Figure 4: A von Bertalanffy growth curve of age estimates (years) combining data derived from this study (blue triangles) with data obtained from Andrews et al., 1999 (red circles).

2. LA-ICP-MS Elemental Profiles

Average polynomial regression lines along ablation transects for 104 otolith samples revealed overall trends in element incorporation for 12 different chemical isotopes (Fig. 5). The elemental profiles for settler and mature specimens exhibited inflection points along average regression lines, suggesting a habitat shift in ontogeny. Most isotopes peak in elemental ratio at the natal origin in the center of the core, except for ^{86}Sr and ^{138}Ba. The average regression line for most isotopes appears to level off once it passes into the mature phase, though a few isotopes indicate an increase in concentration. This observed increase is likely due to the lower sample size at higher lengths skewing the average, however it appears consistent for ^{31}P, ^{86}Sr, and ^{138}Ba. The elemental isotopes ^{55}Mn, ^{86}Sr, and ^{138}Ba all exhibit maxima about 1800 μm along the ablation line, corresponding to specimens at approximately 5-20 years old. The location of this maxima does not appear to be consistent across each individual sample, though it does consistently appear within the bounds of the settlement stage along the track.

Table 3: Summary of elemental ratios (X:^{43}Ca) life stage averages for *C. acrolepis* otoliths. LA-ICP-MS was used to measure elemental ratios for 12 isotopes across otolith transversal sections.

Summary ^{43}Ca Ratio Life Stage Averages

Isotope ($X/^{43}Ca$):	^{7}Li (µmol/mmol)	^{11}B (mmol/mmol)	^{24}Mg (mmol/mmol)	^{26}Mg (mmol/mmol)	^{31}P (mmol/mmol)	^{55}Mn (mmol/mmol)	^{63}Cu (µmol/mmol)	^{65}Cu (µmol/mmol)	^{66}Zn (µmol/mmol)	^{86}Sr (mmol/mmol)	^{138}Ba (µmol/mmol)	^{208}Pb (µmol/mmol)
Larvae	23.483	0.042906	0.29507	0.35081	0.29567	0.0047417	15.126	16.434	51.403	3.1649	6.1892	0.11016
Settler	13.318	0.032102	0.13533	0.14255	0.26428	0.0025565	4.1319	4.7467	14.196	3.8801	8.3644	0.088608
Mature	15.42	0.031164	0.12493	0.13517	0.26053	0.0053443	5.3304	5.9552	19.267	3.5506	6.9265	0.074181
n	81	83	88	89	102	97	95	93	98	102	102	83

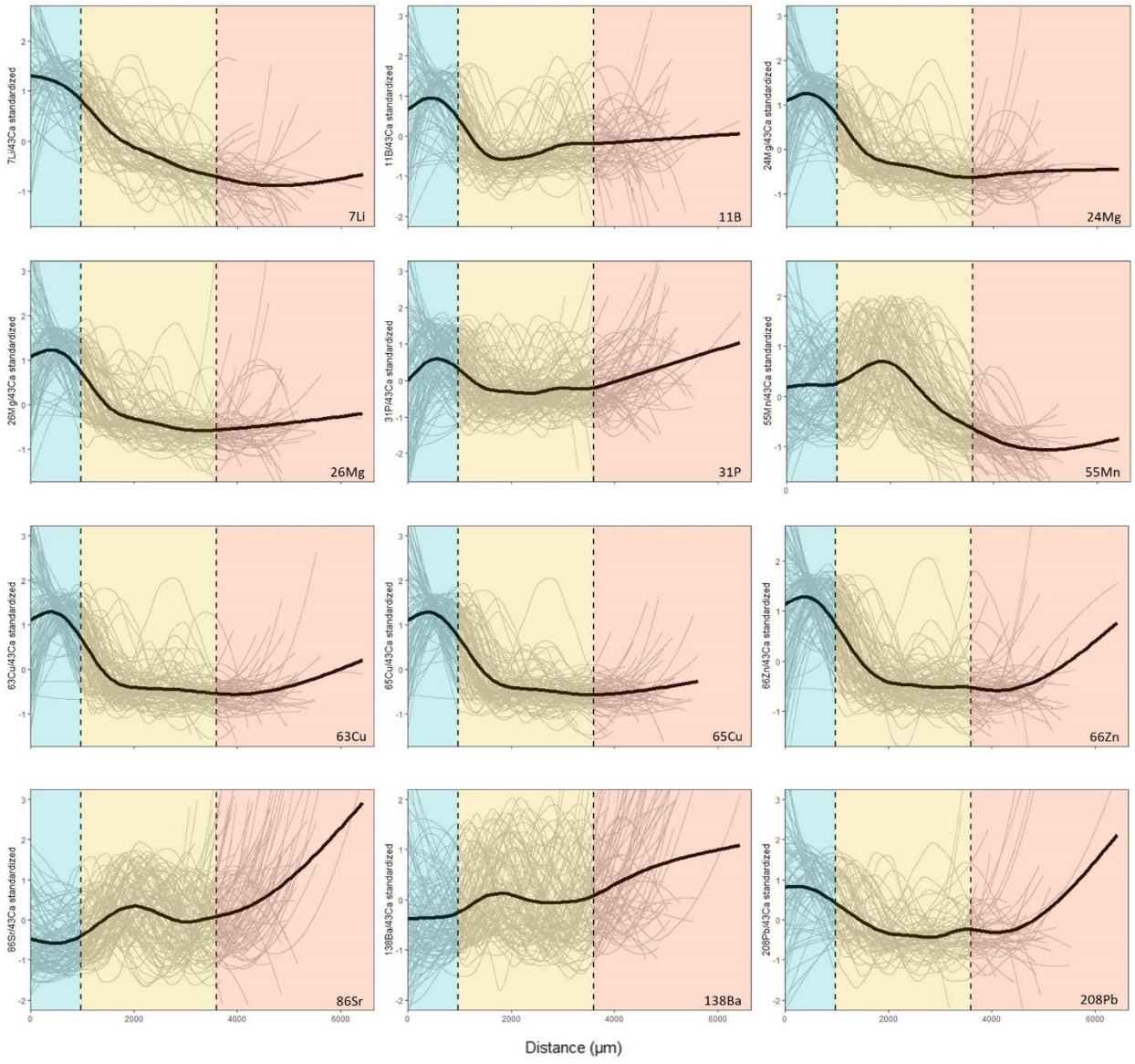

Figure 5: Standardized average otolith elemental ratios fitted with a polynomial regression (n=104). Data was standardized using a z-score normalization. Grey lines indicate elemental ratios for individual samples. Blue, yellow, and red shaded areas indicate larval, settler, and mature life stages, respectively.

3. Life Stage Analysis

Box-and-whisker plots of average elemental ratios for each life stage reflect overall trends depicted in the life history profiles (Fig. 6; Table 3). ^{7}Li, ^{24}Mg, ^{26}Mg, ^{63}Cu, ^{65}Cu, and ^{66}Zn all exhibit a clear decrease in overall elemental ratio from one life stage to the next. Box plots for ^{11}B, ^{31}P, and ^{208}Pb exhibited increased ratios during the larval stage, but no clear differences

between settlement and maturity. ^{86}Sr and ^{138}Ba both increased with each subsequent life stage. ^{55}Mn is distinct from the other elements as we observed a clear peak during the settlement stage followed by a reduction during the adult stage.

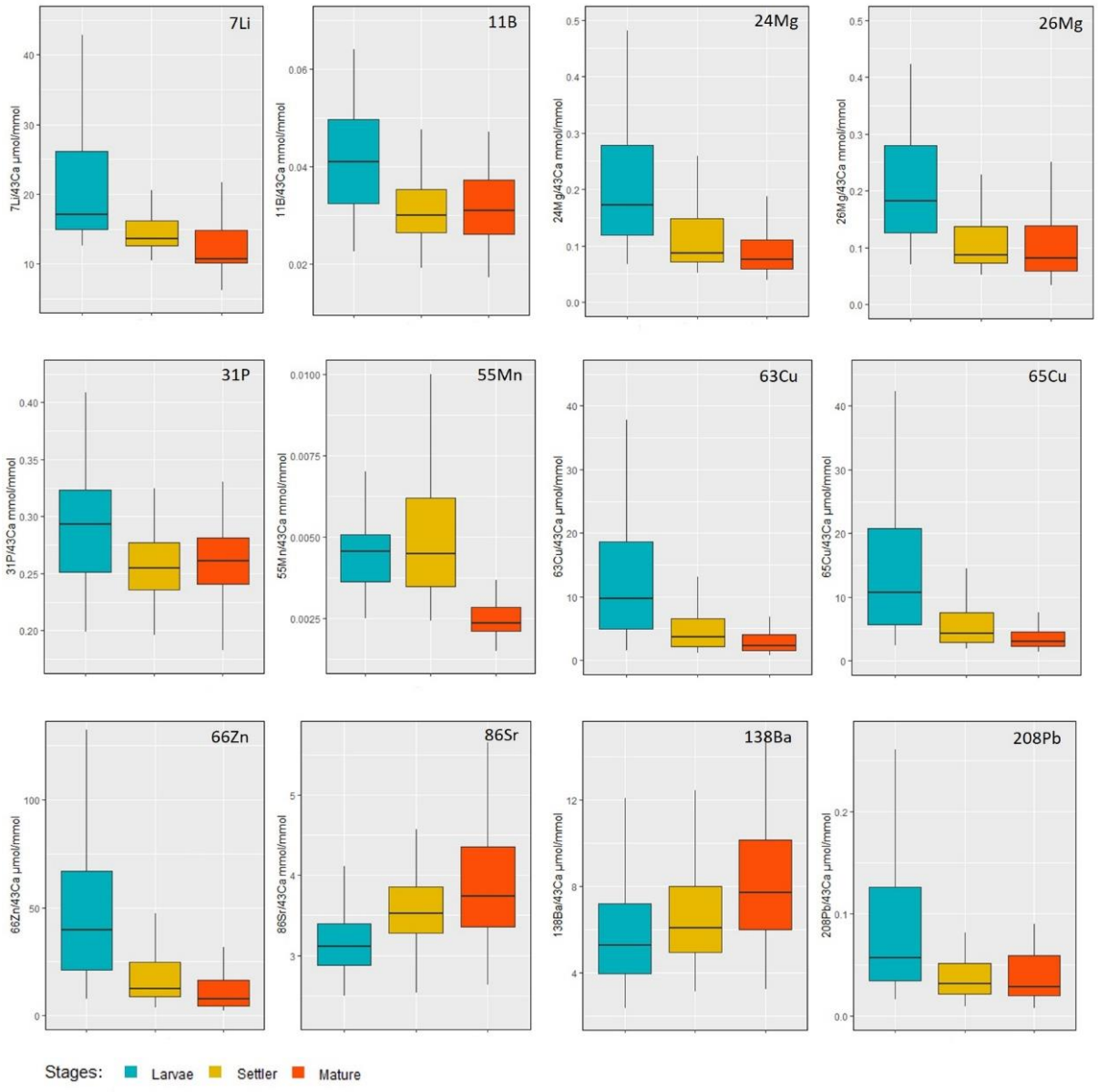

Figure 6: Box-and-whisker plots of average ratios between life stages for each isotope (n=104). Blue, yellow, and red boxes indicate larval, settler, and mature life stages, respectively.

A principal component analysis (PCA) was employed for all fish otoliths, using the average elemental ratio of the three life stages (larvae, settler, and mature) to examine elemental trends across ontogeny. The PCA biplot of the first two dimensions (PC1: 44.6%; PC2: 13.3%) shows the influence of each isotope with the average life stage isotopic ratio plotted (Fig. 9) Average life stage groupings clustered somewhat well, with the larval stage exhibiting the highest amount of variance. Despite some overlap, larval stages were distinct from settlement and maturity, which clustered together. The PC1 primarily explained variability for the larval stage with slight skewing from ^{208}Pb and ^{55}Mn. Conversely, the PC2 primarily explained variability for settler and mature fish and was most influenced by ^{86}Sr and ^{138}Ba. The settler stage appears to represent an intermediary phase between the other two stages, with positive PC1 and PC2 trends, potentially corresponding to intermediate depth strata between larval fish at the surface and mature fish at depth.

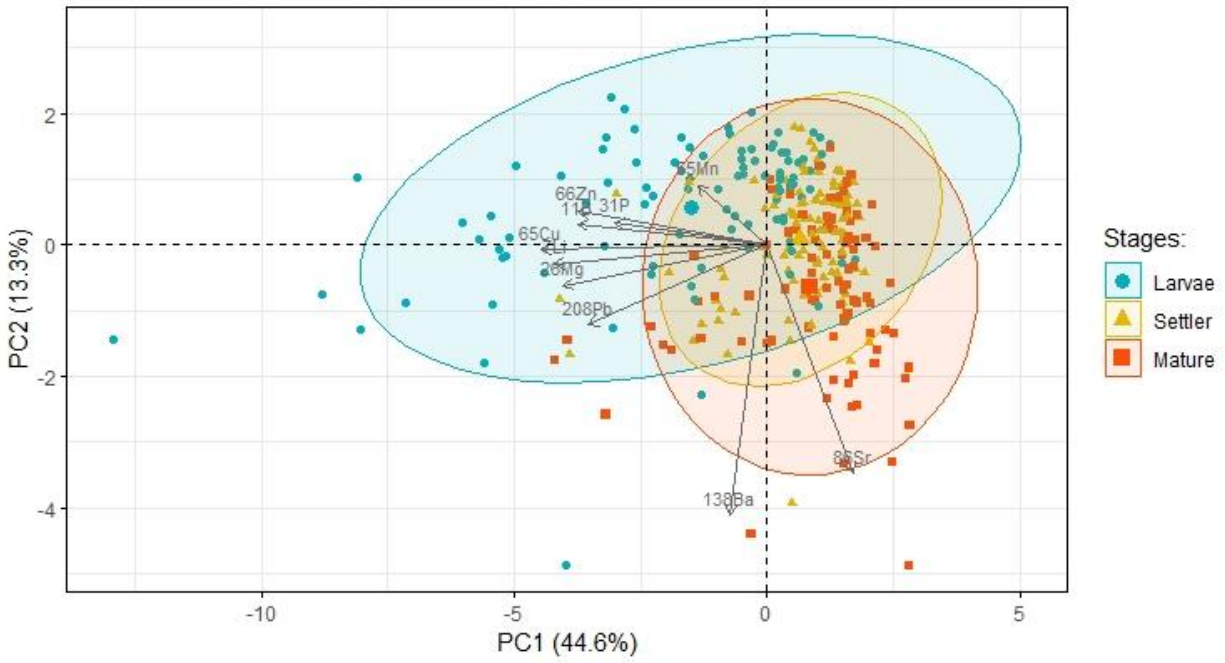

Figure 7: PCA biplot of average isotope ratios among life stages for 10 elemental isotopes (n=104). PC1 = 44.6%; PC2 = 13.3%. Blue circles, yellow squares, and red triangles indicate larval, settler, and mature stages, respectively for an individual. The largest point of each respective life stage indicates the group mean and is surrounded by an 95% confidence ellipse.

4. Spatial Variation

Between the two location groupings— Baja California and Isla Guadalupe— 7 elemental ratios were determined to differ significantly (Table 4). Box plots of average elemental ratio between regions showed the trends for each isotope (Fig. 8). ^{7}Li, ^{26}Mg, ^{63}Cu, and ^{208}Pb exhibited higher average elemental ratios and variance in Isla Guadalupe whereas ^{11}B, ^{55}Mn, ^{86}Sr were higher in Baja, and exhibited similar variances between the two locations.

A PCA of average elemental ratios across individual otoliths collected between these locations featured a similar pattern to the previous PCA incorporating life stages (PC1=44.9%; PC2=13.9%). The position of individual fish within the PCA plot is determined mainly by the PC1 axis and most element variables. Alongside ^{138}Ba and ^{86}Sr, ^{55}Mn had a strong influence on the PC2 axis (Fig. 9). Despite high overlap between location groupings, fish otoliths collected off Baja varied positively with PC1 and negatively with PC2. A secondary PCA plot, this time clustering groups based on k-means clustering rather than location data, accurately reclassified 62.50% of all samples with 32.45% of samples off Isla Guadalupe and 81.48% of samples off Baja California (Fig. 10).

No significant differences in average concentration were found between male and female samples for any of the isotopes ($p > 0.05$).

Table 4: Summary of t-tests between collection sites off Isla Guadalupe, Mexico and the Baja California Peninsula based on the average ^{43}Ca ratio of each isotope. Significant p-values less than an α value of 0.05 are underlined.

Summary of Location Analysis (t-test)													
Isotope:	^{7}Li	^{11}B	^{24}Mg	^{26}Mg	^{31}P	^{55}Mn	^{63}Cu	^{65}Cu	^{66}Zn	^{86}Sr	^{138}Ba	^{208}Pb
p-value	0.00548	0.03683	0.05838	0.02267	0.73367	0.00346	0.02759	0.10806	0.42061	0.0065	0.38689	0.02024
n (Baja)	25	25	24	25	34	33	30	29	32	34	34	21
n (Isla Guadalupe)	44	47	50	50	52	48	50	50	50	53	52	49
n (Total)	69	72	74	75	86	81	80	79	82	87	86	70

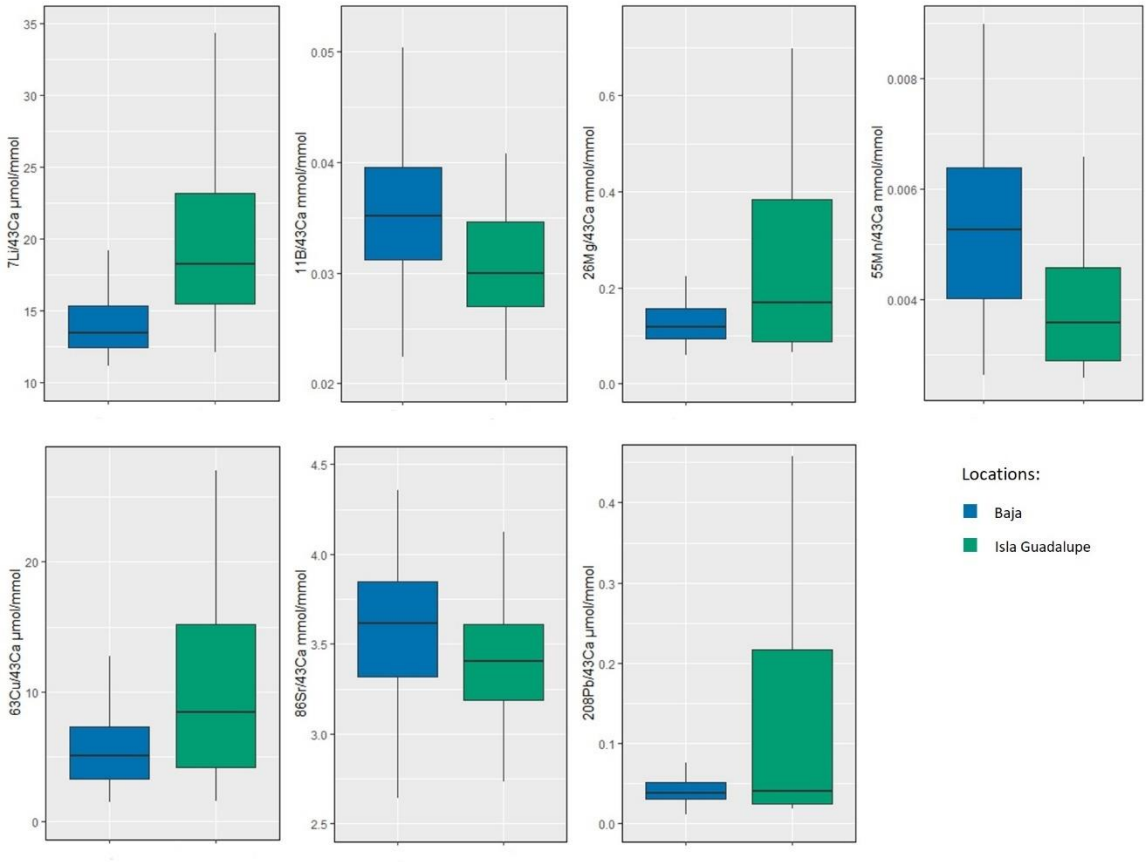

Figure 8: Box-and-whisker plots of average ^{43}Ca ratio between samples collected near Isla Guadalupe or Baja for isotopes determined to be significantly different based on a t-test (n=89). Blue boxes indicate samples collected off Baja, whereas green boxes indicate samples collected near Isla Guadalupe.

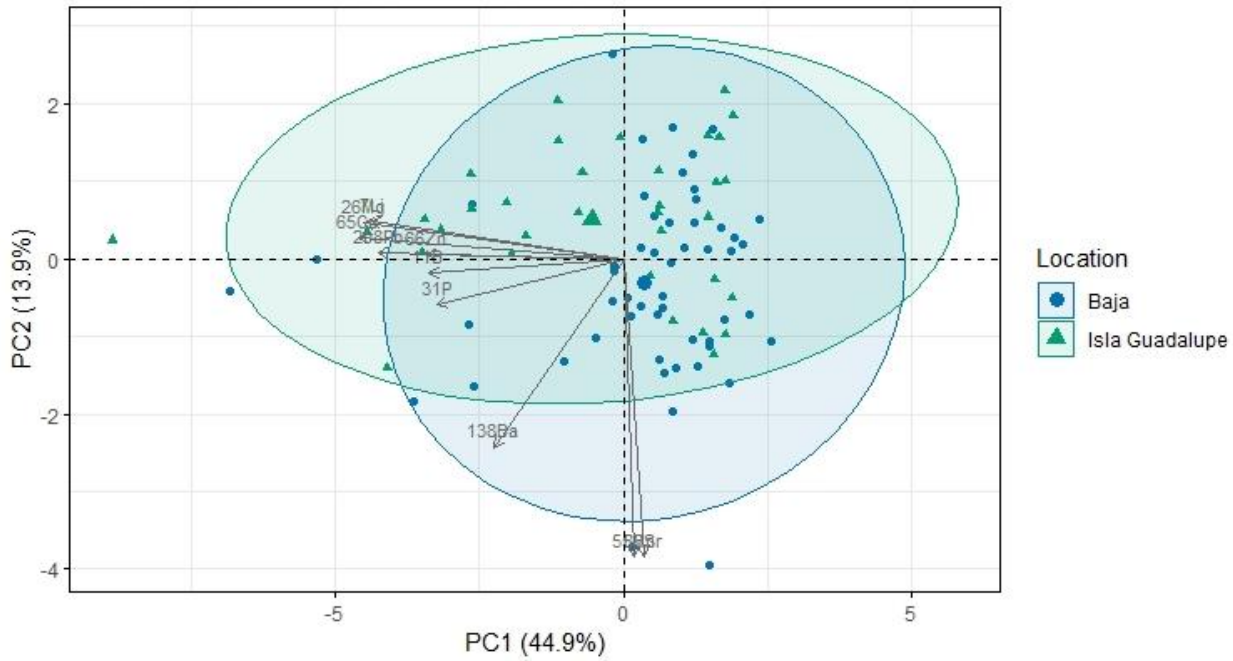

Figure 9: PCA biplot of average element ratios between locations for 10 elemental isotopes (n=89). PC1 = 44.9%; PC2 = 13.9%. Blue circles indicate samples collected offshore of Baja California and green triangles indicate samples collected near Isla Guadalupe. The largest point of each location indicates the group mean and is surrounded by an 95% confidence ellipse.

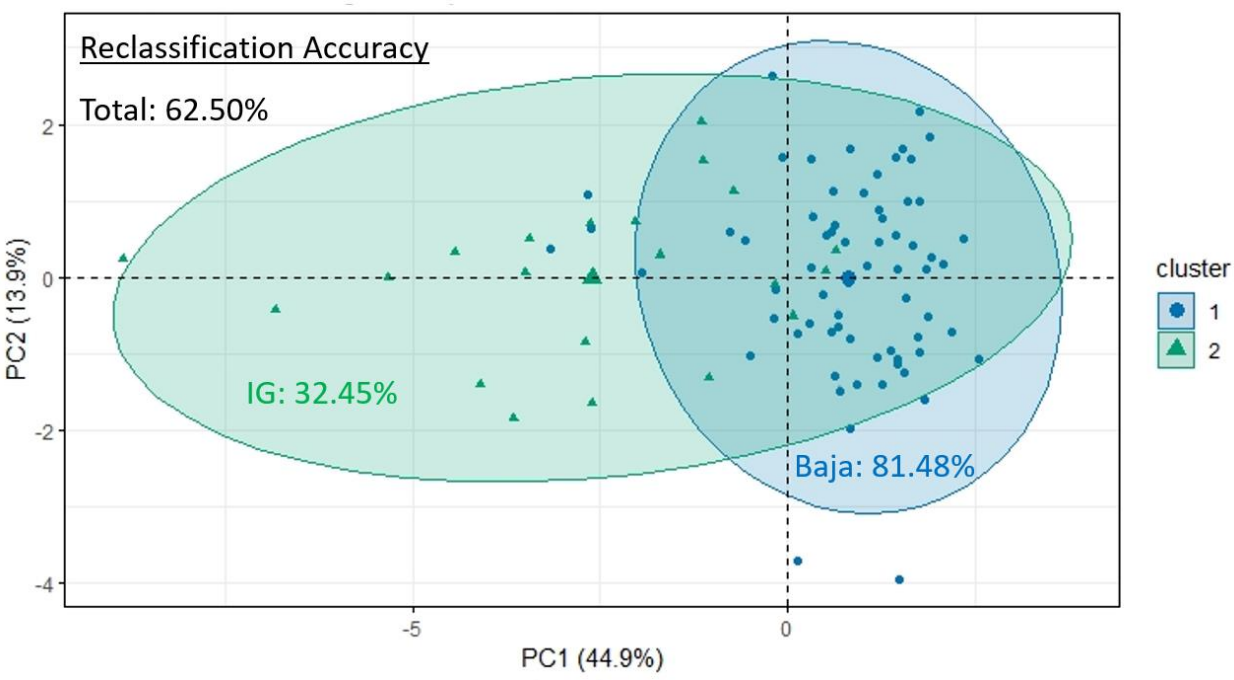

Figure 10: PCA of average element ratios based on k-means clustering for 10 elemental isotopes (n=89). PC1 = 44.9%; PC2 = 13.9%. The largest point of each cluster indicates the group mean and is surrounded by an 95% confidence ellipse. Clusters accurately reclassified 62.50% of all samples; 32.45% of samples off Isla Guadalupe and 81.48% of samples off of Baja California.

DISCUSSION

Studies evaluating otolith morphology and dimension for *C. acrolepis* are limited, though microchemical analysis has been identified as a more efficient means of classification in roundnose grenadier (Longmore et al., 2010). Reliable age and growth estimates for deep sea fish are difficult to achieve due to their long lives and temperature-stable environment. However, age estimates for this sample set are very consistent with previous age and growth study for this species (Fig. 4, Andrews et al., 1999). The inclusion of older and larger specimens with this previous dataset further strengthens the credibility of our growth parameters and growth ring aging method found in *C. acrolepis* otoliths. The lack of seasonal temperature variability in the deep sea suggests that this clear annual growth pattern is the result of mechanisms related to seasonal feeding activity and benthic-pelagic coupling rather than shifts in metabolic rates due to temperature. This is consistent with the hypothesis that grenadier populations are sustained by the seasonally mediated supply of carrion to deeper waters (Bailey et al., 2006, Drazen et al., 2012).

Physiological activity in *C. acrolepis* is expected to decline with age as metabolism and growth slow and individuals migrate to deeper waters. Our results are mostly consistent with this hypothesis. Chemical isotopes that have been related to physiological activity are ^{31}P, ^{63}Cu, ^{65}Cu, and ^{66}Zn (Thomas et al., 2017). The elevated ratios of these isotopes closer to the natal origin have been previously observed and are often related to elevated protein concentrations in the otoliths of younger individuals (Fig. 5, Ruttenberg et al., 2005; Heimbrand et al., 2020). This observation could also be an indicator of increased metabolic activity and somatic growth early in life, which is consistent with the observed growth curve. The elements associated with physiology all decline with distance, reflecting a decrease in their metabolic activity with age.

The slight increase of ^{31}P ratios in the mature phase, however, contradicts this, as phosphorus is also thought to be regulated by metabolic activity. The discrepancy could be accounted for due to the tendency of some element ratios increase closer to the edge of the section, observed in isotopes ^{63}Cu, ^{65}Cu, ^{66}Zn, ^{86}Sr, ^{138}Ba, and ^{208}Pb. The element Mg has exhibited seasonal patterns in some fishes, though it is less clear in species with slower metabolisms (Limburg et al., 2018). This is consistent with our findings, as ^{24}Mg and ^{26}Mg both fail to show any clear or consistent seasonal patterns in *C. acrolepis*, which features a slow metabolism and extended lifespan as adaptations to the deep sea. The gradual decline in ^{66}Zn ratio with age is consistent with patterns observed in roundnose grenadier (*Coryphaenoides rupestris*) in the North Atlantic (Longmore et al., 2011).

Variation in environment for *C. acrolepis* across lifespan is expected to be observable within otolith element ratios. Isotopes ^{7}Li, ^{11}B, ^{86}Sr, ^{138}Ba, and ^{208}Pb are all evidenced to be environmentally mediated within otoliths (Sturrock et al., 2012; Cavole et al., 2020). With *C. acrolepis* exhibiting a downward ontogenetic vertical migration across lifespan, element ratios along the ablation track for elements associated with the environment are expected to mimic element depth profiles in the water column. However, for the measured environmentally mediated elements, the similarity between ambient concentrations and observed otolith profiles is unclear (Bruland, 1983). Measured ^{7}Li, ^{11}B, and ^{208}Pb ratios have patterns similar to the physiologically mediated elements, however, these isotopes are typically only present in the salt fraction of otoliths, indicating strong environmental influence (Thomas et al., 2017). The overall decline of these ratios across ablation distance is not reflected in depth profiles for their respective elements in the Pacific, which are mostly uniform (Schaule & Patterson, 1981; Stoffyn-Egli et al., 1984; Uppstrom, 1974). However, the increased elemental ratios for ^{7}Li, ^{11}B,

and ^{11}Pb are reflective of the increased ambient concentrations of these elements closer to the surface. In addition, the gradual increase of ^{86}Sr and ^{138}Ba with ablation distance appears to mirror the steady increase of both elements with depth in the Pacific (Chan et al., 1976, de Villiers, 1999). Sr and Ba are two of the most studied elements for reconstructing environment in otolith microchemical analyses, since they are primarily influenced by ambient concentrations (Heimbrand et al., 2020). The isotopes ^{86}Sr and ^{138}Ba are the primary variables influencing the PCA2 axis along which the mature stage diverges slightly from settlement (Fig. 7). The steady increase of Sr and Ba into maturity suggests a shift into a higher ambient concentration environment as *C. acrolepis* ages. These observed values could be in response to increased salinity, though attempts to relate otolith element concentrations directly to salinity have only yielded slight correlations for both Sr and Ba. Previous studies have used ^{86}Sr and ^{138}Ba to monitor migrations between areas of different salinities (Walther & Limberg, 2012). Salinity has been shown to increase slightly with depth in northern Baja, though whether this shift is significant enough to influence otolith Sr and Ba ratios is uncertain (Papiol et al., 2017). This relationship would be consistent with *C. acrolepis* ontogenetic vertical migration.

The elevated ratios observed for Mn, Sr, and Ba isotopes following settlement suggests a shift in environment during settlement (Fig. 5). Amongst individuals, these ratios peak at varying distances along the ablation track, though all maxima fall within the bounds of settlement estimates. The variation between samples could be explained by differences in timing of settlement or otolith shape. *C. acrolepis* ontogenetic migration along the continental slope across lifespan indicates that a hydrographic feature is encountered within the water column. The Oxygen Minimum Zone (OMZ) could potentially explain this observation, since previous studies have related elevated Mn ratios to migrations into hypoxic environments in other fishes such as

arapaima, cod, and whitefish (Limburg & Casini et al., 2018, Hüssy et al., 2021). However, attempts to observe this pattern experimentally have only shown slight increases in Mn in relation to hypoxia (Jiang et al., 2022). The OMZ is more pronounced in the southern California bight off Baja, typically found between 400-600 m depth (Papiol et al., 2017). The maxima found in the settlement stage could reflect this depth range during *C. acrolepis* vertical migration. However, Sr and Ba have not been shown to have very strong correlations to hypoxic environments in comparison to Mn, generating uncertainty for the exact cause of the observed maxima in the settlement stage for the three isotopes. Other possibilities for this observation include the effect of the salinity maximum, there being an intermediary habitat during or before settlement, or perhaps it reflects the sudden shift in *C. acrolepis* environment from pelagic larvae to demersal bottom feeders.

Differences in island activity and proximity to the coast between collection sites could have yielded observed differences in otolith elemental ratios. A bulk evaluation of average elemental ratio data through PCA shows a high amount of overlap between the two location groupings, indicating high connectivity (Fig. 9). Similar to how the mature stage separates in our life stage analysis, ^{86}Sr and ^{138}Ba are the primary drivers of difference between the two groups, which suggests that connectivity is higher during larval and settlement stages as opposed to maturity. Studies into larval dispersion within Baja California and the Southern California Bight indicate heterogenous and localized patterns in connectivity (Selkoe et al., 2007; Watson et al., 2010). While our data does not reflect these patterns, our analysis fails to include many of the physical factors at play and the sources of our samples in the larval stage are unknown. Overall, there appears to lack any major differences between the collection sites across our isotope data, with k-means clustering only accurately grouping 62.50% of samples due to high overlap (Fig.

10). The increased ratios of ^{7}Li, ^{26}Mg, ^{63}Cu, and ^{208}Pb in samples collected near Isla Guadalupe may be the result of several influences (Fig. 8). Increased Li ratios in shallower, more enclosed waters has been observed in the North Atlantic, however this pattern is not reflected in the other elements (Longmore et al., 2011). Greater ratios of ^{7}Li, ^{26}Mg, ^{63}Cu in samples collected closer to the island indicates that these individuals had generally greater metabolic activity throughout their lifespan. This observation could be the result of higher productivity closer to the coast of Isla Guadalupe causing an increase in metabolic activity. The larger *C. acrolepis* samples were collected off the coast of Isla Guadalupe, possibly for similar reasons. Samples collected further off the coast of Baja featured significantly higher ^{11}B, ^{55}Mn, ^{86}Sr ratios on average, suggesting a difference in environmental parameters. One theory for this result is that these samples were in a higher salinity environment, with the nearshore environment off Isla Guadalupe having greater freshwater input from runoff (Webb et al., 2012). However, it is unlikely whether this would have a significant impact on the salinity or available concentrations of these elements within the deep sea, as near and offshore salinity doesn't vary significantly with depth (Saldías et al., 2019). Perhaps this difference is skewed towards the larval stages of *C. acrolepis*, when individuals are expected to be closer to the surface and observed isotope ratios in otoliths were often higher.

The lack of any observed differences in element ratio between sexes indicates similar life history traits for both male and female *C. acrolepis*. Age and growth study has yielded only slight differences in size and growth rate between sexes (Andrews et al., 1999). Based on our findings, the isotopes observed that are associated with physiological shifts are likely most related to somatic growth and metabolic activity across life stages, rather than reproductive changes.

Further study is necessary to strengthen the observations found in this study. Because samples were collected between 1967-71, they may not reflect patterns that would be observed today. The waters off the coast of Baja California represent the southernmost range of *C. acrolepis* in the eastern Pacific, which may be shifting due to increasing temperatures. In addition, all samples were mature adults between 50.6 to 87 cm, with few juveniles. The use of the measured isotopes as both physiological and environmental tracers for deep-sea fishes in the north Pacific is limited. Procuring stronger relationships to associated proxies for these elements is essential to bolstering our results. Studies into similar ontogenetic vertical migrators or the use of younger samples can be beneficial in determining the exact nature of the observed maxima for ^{55}Mn, ^{86}Sr, and ^{138}Ba. The specific shift in habitat or hydrographic feature that drives this increase in element ratio is uncertain. Experiments observing the effects of hypoxia in related fishes under similar conditions could be used to determine if it is related to the OMZ. More rigorous study using otolith microchemistry to track larval dispersion and connectivity in context of oceanic currents would be valuable. Increasing and fine-tuning our methodologies used to study organisms in the deep sea, where direct observations are difficult, can further the breath of information available to us through both space and time. Microchemical techniques can be applied to any hard accreting structure, both biotic and abiotic, and contribute to the study of various fields, such as geology and paleontology.

Information on deep-sea organisms, particularly those that are commonly found in hypoxic environments, is of critical importance as OMZ's are continually expanding with changes in climate (Stramma et al., 2008). Understanding the life histories of *C. acrolepis* and similar deep-sea fishes is vital to informing proper management and conservation of these ecosystems. Commercial fishing of deep-sea fishes is increasingly common with pelagic fish

stocks continuing to decline from overfishing (Watson et al., 2013). Because many deep-sea fish are ontogenetic vertical migrators, most younger individuals are found in shallower waters. This younger stock could be fished prior to reaching sexual maturity and are unlikely to survive capture if released. Grenadier are currently fished in small numbers in the north Pacific; however, they can be vulnerable if this pressure is increased particularly due to its slow growth rate and reproduction (Groundfish, US West Coast, 2014; Andrews et al., 1999). As top predators, reducing populations of *C. acrolepis* could have significant impacts on the benthic community in the North Pacific. Increasing further study of the deep-sea ecosystem, the largest habitat on Earth, is vital to informing proper marine policy and preserving its integrity.

This work is in preparation for submission to publication in a journal to be decided. Castillo, Adrian; Cavole, Leticia M.; Andrews, Allen H. "Tracing Life History Patterns of Pacific Grenadier (*Coryphaenoides acrolepis*) off Baja California with Otolith Microchemistry" The thesis author was the primary investigator and author of this manuscript.

SUPPLEMENTAL MATERIALS

Life Stage Estimation:

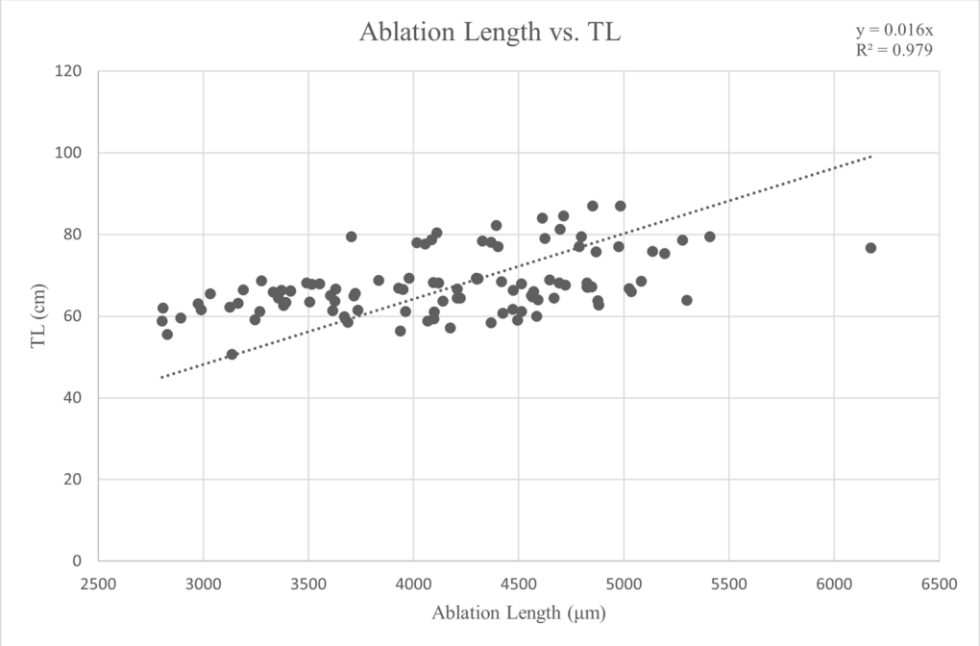

Figure 11: Isometric linear regression between *C. acrolepis* total length and otolith ablation length (n=104). This relationship was used to estimate life stage transitions along ablation transects.

Otolith Parameters:

Across all 118 *C. acrolepis* otoliths, the average width (8.32 ± 0.72 mm), length (15.11 ± 1.43 mm), thickness (3.21 ± 0.35 mm), and weight (0.5272 ± 0.1353 g) varied slightly (Table 5). All otolith metrics were positively related with TL and age. Of the four measurements, otolith weight correlated best (R^2 = 0.2867) with recorded TL values (Fig. 12).

Table 5: Summary of otolith morphology measurements (n = 118). R^2 values indicate linear regressions between TL and the corresponding measurement.

Summary of Otolith Morphology (n= 118)

	TL (cm)	Depth of Collection (m)	Otolith Width (mm)	Otolith Length (mm)	Otolith Thickness (mm)	Otolith Weight (g)
Average ± SD	68.1 ± 7.2	1507 ± 238	8.32 ± 0.72	15.11 ± 1.43	3.21 ± 0.35	0.5272 ± 0.1353
R^2 (TL)	-	0.064	0.2157	0.1968	0.1815	0.2867

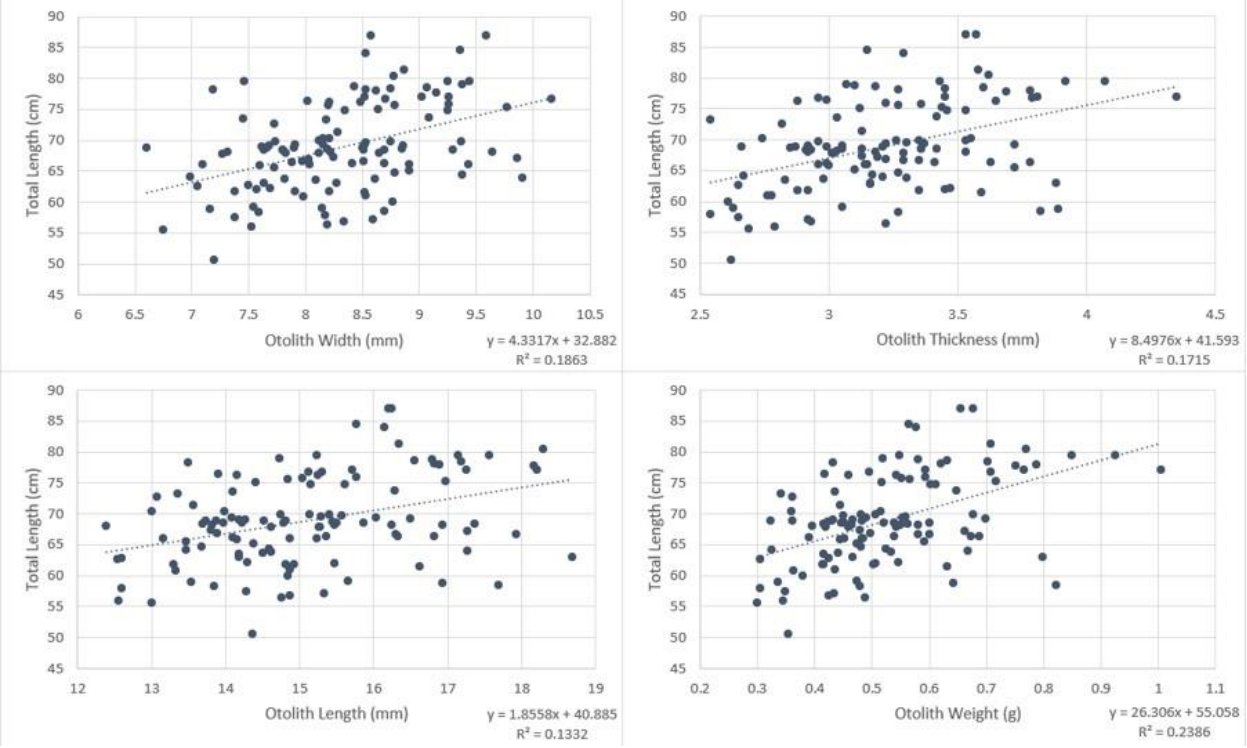

Figure 12: Scatterplots of 4 different otolith morphological parameters (width, thickness, length, weight) in relation to total length for *C. acrolepis* samples (n = 118). Corresponding y-axis equations and R^2 values are included.

LIST OF SUPPLEMENTARY FILES

Castillo_PGMasterDataset.xlsx – Master dataset compiling information on each sample as well as diagrams for the microchemical procedure and a quality control table.

Castillo_PGMicrochem.csv – Calculated elemental ratio data for 104 *C. acrolepis* otolith samples with outliers removed.

Castillo_OSUSlideData.rar – Raw counts per second data from the LA-ICP-MS conducted at the Keck Lab in Oregon State University.

REFERENCES

Andrews, A. H., Cailliet, G. M., & Coale, K. H. (1999). Age and growth of the Pacific grenadier (Coryphaenoides acrolepis) with age estimate validation using an improved radiometric ageing technique. *Canadian Journal of Fisheries and Aquatic Sciences*, *56*(8), 1339-1350.

Bailey, D. M., Ruhl, H. A., & Smith Jr, K. L. (2006). Long-term change in benthopelagic fish abundance in the abyssal northeast Pacific Ocean. Ecology, 87(3), 549-555.

Bruland, K. W. (1983). Chemical oceanography. *Academic Press, London*.

Campana, S. E. (1999). Chemistry and composition of fish otoliths: pathways, mechanisms and applications. *Marine Ecology Progress Series*, *188*, 263-297.

Campana, S. E., & Thorrold, S. R. (2001). Otoliths, increments, and elements: keys to a comprehensive understanding of fish populations?. *Canadian Journal of Fisheries and Aquatic Sciences*, *58*(1), 30-38.

Campana, S. E. (2005). Otolith science entering the 21st century. *Marine and freshwater research*, *56*(5), 485-495.

Cavole, L. M., Andrade-Vera, S., Jarrin, J. R. M., Dias, D. F., Aburto-Oropeza, O., & Barrágan-Paladines, M. J. (2020). Using local ecological knowledge of Fishers to infer the impact of climate variability in Galápagos' small-scale fisheries. *Marine Policy, 121*, 104195.

Chan, L. H., Edmond, J. M., Stallard, R. F., Broecker, W. S., Chung, Y. C., Weiss, R. F., & Ku, T. L. (1976). Radium and barium at GEOSECS stations in the Atlantic and Pacific. *Earth and Planetary Science Letters*, *32*(2), 258-267.

Chen, L., Liu, Y., Hu, Z., Gao, S., Zong, K., & Chen, H. (2011). Accurate determinations of fifty-four major and trace elements in carbonate by LA–ICP-MS using normalization strategy of bulk components as 100%. *Chemical Geology*, *284*(3-4), 283-295.

Cohen, D. M. (1990). Gadiform fishes of the world (Order Gadiformes). An annotated and illustrated catalogue of cods, hakes, grenadier and other gadiform fishes known to date. *FAO species catalogue*, *10*, 1-442.

De Villiers, S. (1999). Seawater strontium and Sr/Ca variability in the Atlantic and Pacific oceans. *Earth and Planetary Science Letters*, *171*(4), 623-634.

Devine, J. A., Watling, L., Cailliet, G., Drazen, J., Durán Muñoz, P., Orlov, A. M., & Bezaury, J. (2012). Evaluation of potential sustainability of deep-sea fisheries for grenadiers (Macrouridae). *Journal of Ichthyology*, *52*(10), 709-721.

Drazen, J. C., Buckley, T. W., & Hoff, G. R. (2001). The feeding habits of slope dwelling macrourid fishes in the eastern North Pacific. *Deep Sea Research Part I: Oceanographic Research Papers, 48*(3), 909-935.

Drazen, J. C., Popp, B. N., Choy, C. A., Clemente, T., Forest, L. D., & Smith Jr, K. L. (2008). Bypassing the abyssal benthic food web: Macrourid diet in the eastern North Pacific inferred from stomach content and stable isotopes analyses. *Limnology and Oceanography*, *53*(6), 2644-2654.

Drazen, J. C., Bailey, D. M., Ruhl, H. A., & Smith Jr, K. L. (2012). The role of carrion supply in the abundance of deep-water fish off California. *PLoS One, 7*(11), e49332.

Fink-Jensen, P., Hüssy, K., Thomsen, T. B., Serre, S. H., Søndergaard, J., & Jansen, T. (2022). Lifetime residency of capelin (Mallotus villosus) in West Greenland revealed by temporal patterns in otolith microchemistry. *Fisheries Research, 247*, 106172.

Gerringer, M. E., Andrews, A. H., Huss, G. R., Nagashima, K., Popp, B. N., Linley, T. D., Gallo, N. D., Clark, M. R., Jamieson, A. J., & Drazen, J. C. (2018). Life history of abyssal and hadal fishes from otolith growth zones and oxygen isotopic compositions. *Deep Sea Research Part I: Oceanographic Research Papers, 132*, 37-50.

Groundfish, US West Coast Grenadier Pacific cod Skates. (2014). *Monterey Bay Aquarium Seafood Watch*.

Heimbrand, Y., Limburg, K. E., Hüssy, K., Casini, M., Sjöberg, R., Palmén Bratt, A.-M., Levinsky, S.-E., Karpushevskaia, A., Radtke, K., & Öhlund, J. (2020). Seeking the true time: Exploring otolith chemistry as an age-determination tool. *Journal of Fish Biology, 97*(2), 552–565. https://doi.org/10.1111/jfb.14422

Hoyer, M. V., Shireman, J. V., & Maceina, M. J. (1985). Use of Otoliths to Determine Age and Growth of Largemouth Bass in Florida. *Transactions of the American Fisheries Society*, *114*(2), 307–309. doi: 10.1577/1548-8659(1985)114<307:uootda>2.0.co;2

Hüssy, K., Krüger-Johnsen, M., Thomsen, T. B., Heredia, B. D., Næraa, T., Limburg, K. E., Heimbrand, Y., McQueen, K., Haase, S., Krumme, U., Casini, M., Mion, M., & Radtke, K. (2021). It's elemental, my dear Watson: validating seasonal patterns in otolith chemical chronologies. *Canadian Journal of Fisheries and Aquatic Sciences*, *78*(5), 551-566.

Hüssy, K., Limburg, K. E., de Pontual, H., Thomas, O. R., Cook, P. K., Heimbrand, Y., Blass, M., & Sturrock, A. M. (2021). Trace element patterns in otoliths: the role of biomineralization. *Reviews in Fisheries Science & Aquaculture, 29*(4), 445-477.

Jiang, S., Hong, P., & Katayama, S. (2022). What is the relationship between hypoxia, water chemistry and otolith manganese content?. *Journal of Fish Biology*.

Jochum, K. P., Weis, U., Stoll, B., Kuzmin, D., Yang, Q., Raczek, I., Jacob, D. E., Stracke, A., Birbaum, K., Frick, D. A., Günther, D., & Enzweiler, J. (2011). Determination of reference values for NIST SRM 610–617 glasses following ISO guidelines. *Geostandards and Geoanalytical Research*, *35*(4), 397-429.

Jones, J., & Hynes, H. (1950). The Age and Growth of Gasterosteus aculeatus, Pygosteus pungitius and Spinachia vulgaris, as Shown by their Otoliths. *Journal of Animal Ecology*, *19*(1), 59-73. doi:10.2307/1571

Lin, H. Y., Shiao, J. C., Chen, Y. G., & Iizuka, Y. (2012). Ontogenetic vertical migration of grenadier revealed by otolith microstructures and stable isotopic composition. *Deep Sea Research Part I: Oceanographic Research Papers*, *61*, 123-130.

Limburg, K. E., Huang, R., & Bilderback, D. H. (2007). Fish otolith trace element maps: new approaches with synchrotron microbeam x-ray fluorescence. *X-Ray Spectrometry: An International Journal*, *36*(5), 336-342.

Limburg, K. E., Wuenschel, M. J., Hüssy, K., Heimbrand, Y., & Samson, M. (2018). Making the otolith magnesium chemical calendar-clock tick: plausible mechanism and empirical evidence. *Reviews in Fisheries Science & Aquaculture*, *26*(4), 479-493.

Limburg, K. E., & Casini, M. (2018). Effect of marine hypoxia on Baltic Sea cod *Gadus morhua*: evidence from otolith chemical proxies. *Frontiers in Marine Science*, *5*, 482.

Longmore, C., Fogarty, K., Neat, F., Brophy, D., Trueman, C., Milton, A., & Mariani, S. (2010). A comparison of otolith microchemistry and otolith shape analysis for the study of spatial variation in a deep-sea teleost, Coryphaenoides rupestris. *Environmental biology of fishes*, *89*(3), 591-605.

Longmore, C., Trueman, C. N., Neat, F., O'Gorman, E. J., Milton, J. A., & Mariani, S. (2011). Otolith geochemistry indicates life-long spatial population structuring in a deep-sea fish, Coryphaenoides rupestris. *Marine Ecology Progress Series*, *435*, 209-224.

Lough, R. G., Pennington, M., Bolz, G. R., & Rosenberg, A. A. (1981). Age and growth of larval Atlantic herring, *Clupea harengus* L., in the Gulf of Maine-Georges Bank region based on otolith growth increments.

Massutí, E., Morales-Nin, B., & Stefanescu, C. (1995). Distribution and biology of five grenadier fish (Pisces: Macrouridae) from the upper and middle slope of the northwestern Mediterranean. *Deep Sea Research Part I: Oceanographic Research Papers*, *42*(3), 307-330.

Matsui, T., Kato, S., & Smith, S. E. (1990). Biology and potential use of Pacific grenadier, Coryphaenoides acrolepis, off California. *Mar. Fish. Rev*, *52*(3), 1-17.

Orlov, A. M., & Tokranov, A. M. (2008). Some ecological and biological features of giant and popeye grenadiers in the Pacific waters off the northern Kuril Islands and southeastern

Kamchatka. *Grenadiers of the world oceans: biology, stock assessment, and fisheries*, *63*, 225-260.

Pacific Coast Groundfish Fishery Management Plan. (2020). *Pacific Fishery Management Council*.

Palace, V. P., Halden, N. M., Yang, P., Evans, R. E., & Sterling, G. (2007). Determining residence patterns of rainbow trout using laser ablation inductively coupled plasma mass spectrometry (LA-ICP-MS) analysis of selenium in otoliths. *Environmental science & technology*, *41*(10), 3679-3683.

Pannella, G. (1971). Fish otoliths: daily growth layers and periodical patterns. *Science*, *173*(4002), 1124-1127.

Papiol, V., Hendrickx, M. E., & Serrano, D. (2017). Effects of latitudinal changes in the oxygen minimum zone of the northeast Pacific on the distribution of bathyal benthic decapod crustaceans. *Deep Sea Research Part II: Topical Studies in Oceanography*, *137*, 113-130.

Priede, I. G., Smith Jr, K. L., & Armstrong, J. D. (1990). Foraging behavior of abyssal grenadier fish: inferences from acoustic tagging and tracking in the North Pacific Ocean. *Deep Sea Research Part A. Oceanographic Research Papers*, *37*(1), 81-101.

Russo, R. E., Mao, X. L., Liu, H. C., Yoo, J. H., & Mao, S. S. (1999). Time-resolved plasma diagnostics and mass removal during single-pulse laser ablation. *Applied Physics A*, *69*(1), S887-S894.

Ruttenberg, B. I., Hamilton, S. L., Hickford, M. J., Paradis, G. L., Sheehy, M. S., Standish, J. D., Ben-Tzvi, O., & Warner, R. R. (2005). Elevated levels of trace elements in cores of otoliths and their potential for use as natural tags. Marine Ecology Progress Series, 297, 273-281.

Saldías, G. S., Sobarzo, M., & Quiñones, R. (2019). Freshwater structure and its seasonal variability off western Patagonia. *Progress in Oceanography*, *174*, 143-153.

Sanborn, M., & Telmer, K. (2003). The spatial resolution of LA-ICP-MS line scans across heterogeneous materials such as fish otoliths and zoned minerals. *Journal of Analytical Atomic Spectrometry*, *18*(10), 1231-1237.

Schaule, B. K., & Patterson, C. C. (1981). Lead concentrations in the northeast Pacific: evidence for global anthropogenic perturbations. *Earth and Planetary Science Letters*, *54*(1), 97-116.

Selkoe, K. A., Vogel, A., & Gaines, S. D. (2007). Effects of ephemeral circulation on recruitment and connectivity of nearshore fish populations spanning Southern and Baja California. *Marine Ecology Progress Series*, *351*, 209-220.

Serre, S. H., Nielsen, K. E., Fink-Jensen, P., Thomsen, T. B., & Hüssy, K. (2018). Analysis of cod otolith microchemistry by continuous line transects using LA-ICP-MS. *GEUS Bulletin*, *41*, 91-94.

Stoffyn-Egli, P., and MacKenzie, F. T., 1984. Mass balance of dissolved lithium in the oceans. *G Geochim. Cosmochim. Acta 48*: 859-872.

Stramma, L., Johnson, G. C., Sprintall, J., & Mohrholz, V. (2008). Expanding Oxygen-Minimum Zones in the Tropical Oceans. *Science*, *320*(5876), 655–658. doi: 10.1126/science.1153847

Sturrock, A. M., Trueman, C. N., Darnaude, A. M., & Hunter, E. (2012). Can otolith elemental chemistry retrospectively track migrations in fully marine fishes?. *Journal of Fish Biology*, *81*(2), 766-795.

Sturrock, A. M., Hunter, E., Milton, J. A., EIMF, Johnson, R. C., Waring, C. P., & Trueman, C. N. (2015). Quantifying physiological influences on otolith microchemistry. *Methods in Ecology and Evolution*, *6*(7), 806-816.

Thomas, O. R., Ganio, K., Roberts, B. R., & Swearer, S. E. (2017). Trace element–protein interactions in endolymph from the inner ear of fish: implications for environmental reconstructions using fish otolith chemistry. *Metallomics*, *9*(3), 239-249.

Tuponogov, V. N. (1997). Seasonal migrations of the grenadier Coryphaenoides pectoralis in the Sea of Okhotsk and contiguous waters. *Russ. J. Mar. Biol.*, *23*, 314-321.

Tuponogov, V. N., Orlov, A. M., & Kodolov, L. S. (2008). The most abundant grenadiers of the Russian Far East EEZ: distribution and basic biological patterns. In *Grenadiers of the World Oceans: Biology, Stock Assessment, and Fisheries, Am. Fish. Soc. Symp* (Vol. 63, pp. 285-316).

Uppstrom, L. R. (1974). The boron/chlorinity ratio of deep-sea water from the Pacific Ocean. *Deep Sea Res.*, *21*, 161-162.

Walther, B. D., & Limburg, K. E. (2012). The use of otolith chemistry to characterize diadromous migrations. *Journal of Fish Biology*, *81*(2), 796-825.

Watson, J. R., Mitarai, S., Siegel, D. A., Caselle, J. E., Dong, C., & McWilliams, J. C. (2010). Realized and potential larval connectivity in the Southern California Bight. *Marine Ecology Progress Series*, *401*, 31-48.

Watson, R. A., & Morato, T. (2013). Fishing down the deep: Accounting for within-species changes in depth of fishing. *Fisheries Research, 140*, 63-65.

Webb, S. D., Woodcock, S. H., & Gillanders, B. M. (2012). Sources of otolith barium and strontium in estuarine fish and the influence of salinity and temperature. *Marine Ecology Progress Series*, *453*, 189-199.